scientific reports

Check for updates

OPEN

Synthesis and photophysical investigations of pyridine-pyrazolate bound boron(III) diaryl complexes

Rashid Javaid[1]✉, Aziz Ul Rehman[2,3], Manan Ahmed[4], Mohammad Hashemi Karouei[1] & Nima Sayyadi[1,2]

This study presents the design and synthetic pathway of unsymmetric ligands based on pyridine-pyrazolate scaffold with Donor–Acceptor (D–A) molecular arrays and their boron complexes to achieve a large Stokes shift. Intermolecular charge transfer (ICT) triggered by the uneven molecular charge distribution from electronically dense pyrazolate (donor) part of the ligands to electron-deficient boron centre (acceptor) resulted in a mega Stokes shift up to 263 nm for selected compounds while retaining the characteristic quantum efficiency and chemical stability. The photophysical properties of derivatization of pyrazolate group in the pyridine-pyrazolate scaffold of diaryl boron complexes were explored based on UV–Visible, steady-state and time-resolved fluorescence spectroscopy. An interesting dual emission along with quenching behaviour was also observed for 2-(6-methoxynaphthelene) 5-(2-pyridyl) pyrazolate boron complex (P_5) due to the formation of a twisted intermolecular charge transfer (TICT) state from a locally excited (LE) state rendering it a potential candidate for sensing applications based on H-Bond quenching. In addition, the extended excited state lifetime of the reported compounds compared to classical boron-dipyrromethene (BODIPY) makes them suitable as potential probes for analytical applications requiring a longer excited state lifetime.

Small organic and organometallic fluorescent dyes are vital in the modern world and have applications in a variety of domains such as nanoscience[1], solar energy conversion[2], and biological chemistry[3,4]. Attributes of a successful dye include high absorption coefficient and quantum yields, large Stokes shifts, tunability and high photo and chemical stability[5]. In this regard, organoboron complexes enjoy a great deal of attention due to their unique fluorescence properties and high levels of structural diversity which can be managed by changing the organic ligands involved in coordination[6,7]. Among various types of boron complexes, boron dipyrromethene (BODIPY) are well-known and one of the main fluorescent dye with some excellent properties. For instance, their high fluorescence quantum yields, sharp absorption/emission spectra, tunability, ease of functionalization[8] and chemical stability[9–12]. In addition, the properties of BODIPY have been also found in photodynamic therapy agents[13,14], chemosensors[15,16], solar cells[17,18] and potential to be used as thermal and thermoelectric devices owing to their exceptional thermoelectric effect[19,20]. However, most BODIPY dyes and their derivatives have certain disadvantages such as small Stokes shifts (typically 5–20 nm) due to their rigid structure which are usually responsible for self-quenching and background scattering of its own fluorescent. Secondly, the BODIPY dyes are commonly faint or non-fluorescent in the solid state due to the strong π–π stacking of planar fluorophores[21]. Thus, this deficiency limits their use as a material for comprehensive applications such as biological imaging[22].

A straightforward approach to overcome this problem is the rational design of boron fluorescent dyes with low-symmetry or asymmetric *N,N*-ligands, in particular, desymmetrisation of the standard BODIPY core with a donor–acceptor (D–A) architecture[23]. Notable examples are ketoiminosoindolines, benzothiazole-pyrimidines, carbazole-benzimidazoles, carbazole 2-azoles, benzothiazole-pyrimidines, and pyridyl-enamido-based derivatives. Such an approach has been reported to have not only resulted in large Stokes shifts and solvatochromism

[1]Department of Molecular Sciences, Macquarie University, Sydney, NSW 2109, Australia. [2]ARC Centre of Excellence for Nanoscale Bio Photonics (CNBP), Macquarie University, Sydney, NSW 2109, Australia. [3]Agriculture & Biophotonics Division, National Institute of Lasers and Optronics College, Pakistan Institute of Engineering and Applied Sciences (PIEAS), Islamabad 45650, Pakistan. [4]School of Chemistry, The University of New South Wales, Sydney 2052, Australia. ✉email: rashidjavaid143@gmail.com

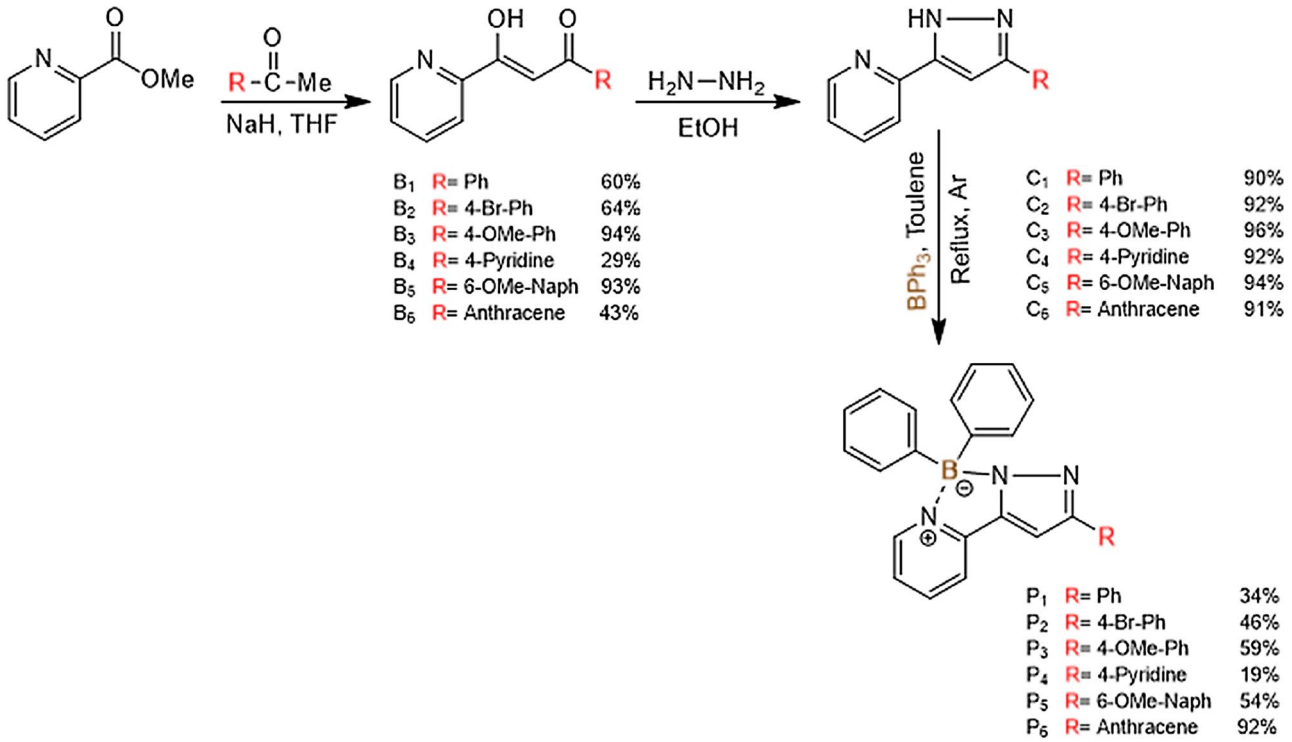

Figure 1. Synthetic route for the pyridine-pyrazolate boron complexes.

but also high luminescence efficiency, the mechanism for the phenomenon was visualized using charge density difference (CDD) recently[24–26]. This is because of the two-photon scaffolds nature of these molecules and their strong intramolecular charge transfer (ICT) in excited states, as a result, their emission wavelength exhibits a large redshift with respect to their environment such as a change in polarity of solvents. However, it is also noted that under a polar environment (physiological condition) D-A type architecture suffers serious twisted internal charge transfer (TICT) and external conversion (EC) which produces severe fluorescence quenching, as a result, high single-to-background ration (SBR)[27–31].

Recently, the synthesis of N-B-N and N-B-O based boron complexes using heterocycle and imido or imine nitrogen or enolate/phenolate oxygen or between two different heterocyclic systems are rapidly growing areas in this field. Because such complexes are a promising candidate for a range of possibilities in terms of structural variation and exhibit a large Stroke shift[32–35]. For instance, Chi and co-workers have previously reported the synthesis of boron compounds based on the pyridine-pyrazolate ligands scaffold by adopting a pull–push approach and observed interesting solvent-dependent properties[36]. However, herein a distinct methodology was adopted to execute efficient fluorescent boron complexes based on pyridine-pyrazolate ligands with a D-A architecture through the gradual increase of electron density on the derivatized pyrazolate (donor) side of the ligands with the pyridyl site acting as the acceptor using literature protocols[37]. The effect of varying electronic density on the ligand scaffold through the inclusion of different functional groups is studied by UV–Visible (UV–Vis) absorption, excitation/ emission, and excited-state lifetimes of the resulting fluorophore in different solvents.

Bearing in mind the importance of fluorescent dyes, herein we have designed and synthesised a new family of boron complexes based on pyridine-pyrazolate ligands with improved features including large Stokes shift, high emission efficiency, extended excited-state lifetime and solvatochromism, compared to classical BODIPY dyes.

Results and discussion

Synthesis and characterization. The three-step synthetic route used in this work for the preparation of the pyridine-pyrazolate ligands scaffold and their biphenyl boron complexes is summarized in Fig. 1. P_1–P_6 were synthesised utilizing optimized conditions[38] via a 1,3-diketone pathway using Claisen condensation[36]. The methyl ester of picolinic acid was refluxed with the corresponding ketone using sodium hydride (NaH) as a catalyst. Tetrahydrofuran (THF) was dried prior, as the synthesis was found to be moisture sensitive[1,39]^{1}H nuclear magnetic resonance (NMR) analysis of 1,3-diketones (B_1-B_6) inferred that they exist in keto-enolic tautomeric forms, the enolic form was found to be dominant (a distinct enolic proton at around 16 ppm of enolic and methine (CH) as singlet). Pyridine-pyrazolate ligands were prepared by refluxing 1,3-diketones with hydrazine hydrate. The reaction was efficient with yields ranging from 90 to 100%. Finally, the ligands were coordinated by refluxing with BPh_3 in toluene until, they were consumed completely, as monitored by thin layer chromatography (TLC) analysis. The resulting boron complexes were isolated using column chromatography (silica gel) as white (P_1, P_2, P_4, P_5) and yellow (P_3, P_6) crystalline solids in yields ranging from 19 to 92%.

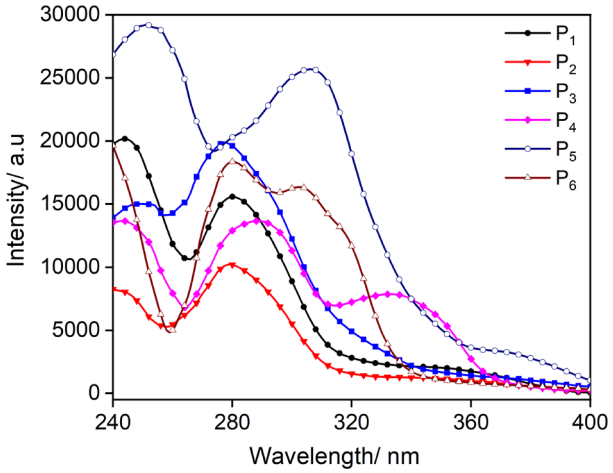

Figure 2. UV–Vis absorption spectra of P_1–P_6 in CH_2Cl_2 (25 μM) at 298 K.

Absorption (CH_2Cl_2)			Emission				
Compound	λ_{abs}[nm](ε[M^{-1} cm^{-1}])[a]	τ_o (ns) [a, b]	$\lambda_{em[nm]}$ [a]	Stokes Shift [nm] [a]	Φ_F [a]	$K_{nr[ns]}$ [c]	$K_{r[ns]}$ [c]
P_1	244 (20,300)	12.94	463	219	0.50	0.039	0.039
P_2	278 (10,200)	6.96	461	183	0.64	0.052	0.091
P_3	277 (19,900)	10.43	508	231	0.71	0.028	0.068
P_4	288 (13,700)	8.83	433	145	0.62	0.044	0.07
P_5	250 (29,400)	10.62	370,513	120, 263	0.43	0.054	0.04
P_6	280 (18,400)	10.05	486	206	0.71	0.029	0.071

Table 1. Photophysical properties of synthesized boron complexes. [a]λ_{abs} (absorption), λ_{em} (emission) measured in CH_2Cl_2 at 25 μM and room temperature. Uncertainty for λ_{abs} and λ_{em}: ± 1 nm. Uncertainty for τ_o ± 0.3 ns. [b]Lifetimes measured using CH_2Cl_2 under an inert atmosphere. Uncertainty for τ_o: ± 0.1 ns. [c]Rates constants of radiative (k_r) and non-radiative (k_{nr}) decay calculated using the formula $K_r = \frac{\Phi F}{\tau o}$ and (Φ_F stands for emission efficiency) τ_o refers to lifetime. $K_{nr} = \frac{(1-\Phi F)}{\tau o}$.

The preliminary confirmation of product formation was made by comparing the ^{1}H NMR of the product with that of the precursor 1,3 diketone (B_1–B_6) through the characteristic protons of the diketone *i.e.,* enolic and methine. Upon pyrazole ring (C_1–C_6) formation the enolic proton disappeared, and a new broad peak appeared at around 12 ppm indicative of the –NH functional group. Further shifting of ^{1}H resonance peaks up field, consistent with the replacement of the electronegative oxygen with comparatively less electronegative nitrogen was observed. The chelation of the ligand with boron was marked by the disappearance of –NH and further up field shift in the proton resonance signals upon formation of the complex. The purity of the final compounds was further confirmed by ^{13}C NMR and high-resolution mass spectroscopy (HRMS) analysis (ESI-appendix).

The boron complexes displayed stability towards the air, moisture and room temperature for extended periods and no changes were observed based on the NMR and UV–Vis analysis. All the complexes were soluble in organic solvents including dichloromethane (DCM), THF, ethyl acetate (EA), chloroform, methanol, ethanol, acetone, benzene, pyridine, and toluene. P_1–P_4 have been reported elsewhere for their usefulness as Raman reporter molecules[40].

Photophysical properties. To evaluate the potential of the synthesised dyes as fluorescent probes, UV–Vis absorption and fluorescence studies were carried out in CH_2Cl_2 at a concentration of 25 μM and 298 K, depicted in (Fig. 2) and summarized in Table 1. The parent compound P_1 exhibited two distinct transitions, a higher energy transition observed at 244 nm and a moderately strong peak at slightly lower energy around 280 nm with a higher molar absorption coefficient (ε = 20,300 M^{-1} cm^{-1}). The transitions can be tentatively assigned to the planar pyridyl pyrazolate ligands where the highest occupied molecular orbital (HOMO) mainly resides on pyrazolate and the lowest unoccupied molecular orbital (LUMO) on the pyridine moiety[36,38]. The absorption profiles do not vary significantly for complexes P_1–P_3 and P_5 due to their similar framework, however, P_4 and P_6 displayed different absorption behaviour having two slightly red-shifted bands (P_4 = 249, 288 nm, P_6 = 246, 280 nm) compared to the parent complex, and also an additional third band at 335 nm and 310 nm, respectively due to the presence of pyridine and anthracene in the ligand scaffold[41,42]. While, all compounds displayed a negligible substitution effect however no regular trend was observed. Similar anomalous behaviour was observed in ε values and the reason for the shifting of the ε values is unclear[43–45].

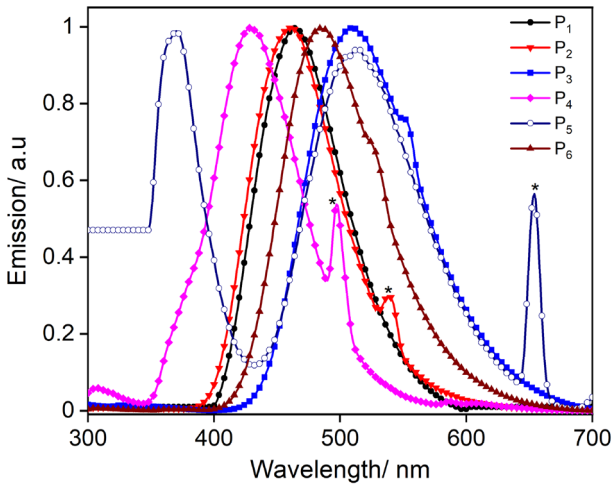

Figure 3. Normalized emission spectra of P_1–P_6 in CH_2Cl_2 (25 μM) at 298 K. Scattering is marked as *.

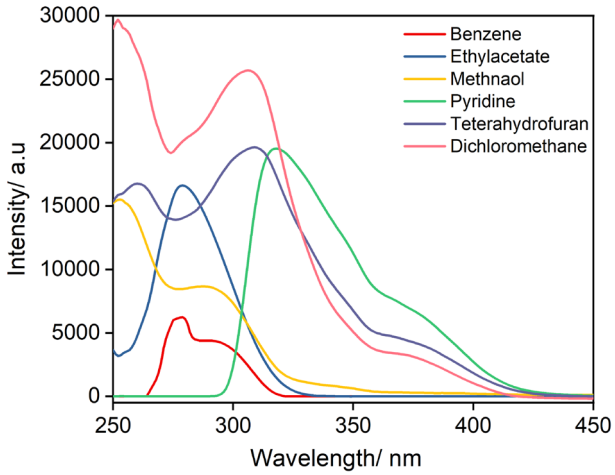

Figure 4. UV–Vis absorption spectra of P_5 (25 μM) as a function of solvent s at 298 K. Spectra zeroed at 450 nm, even for compounds with significant scattering apparent.

The emission profiles observed for all synthesised compounds (P_1–P_6) ranged from violet to green region of the electromagnetic spectrum (428 nm to 513 nm) Fig. 3. The emission maxima of 463 nm for P_1 were found in accordance with the previously reported emission values for the compound[36,38]. The effect of substitution in the emission profiles was more prominent compared to the behaviour observed in the UV–Vis absorption spectra, as negligible changes for P_2 were observed compared to the parent compound, while P_3 and P_5 displayed a significant red shift due to electron-donating nature of –OMe group. A dual emission behaviour was observed for P_5. All the tested compounds displayed larger Stokes shifts ranging from 143 to 263 nm, than that typically found in the case of BODIPY's (5–20 nm)[9] (Fig. 3).

Large Stokes shifts are usually dependent on solvent re-orientation and excited state conformational changes *i.e.,* the geometry differences between the ground state (S_0) and the energy-minimized first excited state (S_1) or both[28,46,47]. In principle, unsymmetrical fluorescent compounds exhibit energetically distinct S_0 and S_1 states and ICT contributes to the large Stokes shift[48]. The nearly planar architecture of the synthesised compounds and their unsymmetric nature are potentially responsible for the emergence of large Stokes shifts, with pyrazolate acting as an electron donor to electron-deficient pyridyl centre facilitating ICT. The relative photoluminescence quantum yields (PLQY) of these compounds were measured using quinine hemisulfate monohydrate as a standard. All the compounds show high quantum yields with P_3 and P_6 displaying the highest value of 0.71. The lowest emission efficiency and highest non-radiative decay were observed for P_5 (Table 1).

Further insight into the fluorescence properties was obtained by time-resolved fluorescence spectroscopy. All the excited-state lifetimes displayed monoexponentially decay with lifetimes ranging from 6.96 to 12.94 ns in DCM compared to the classical BODIPY dyes having a lifetime of 2 ns[9]. All tested compounds except P_5 displayed no effect of solvents on their photophysical properties.

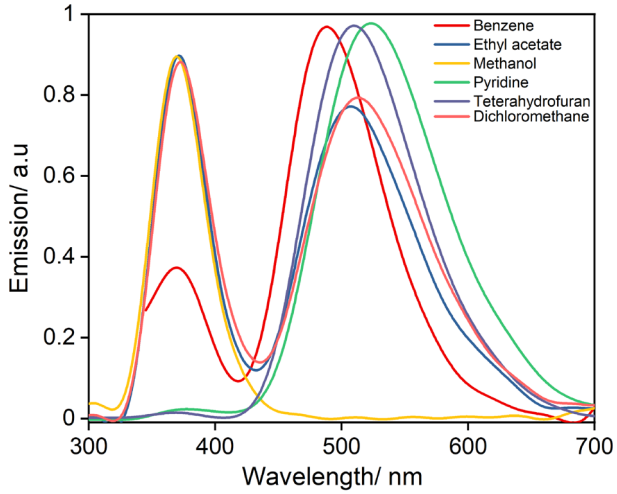

Figure 5. Normalized emission spectra of P_5 (25 μM) as a function of solvent at 298 K.

Absorption (CH_2Cl_2)			Emission			
Solvent	$\lambda_{abs[nm]}(\varepsilon[M^{-1}\ cm^{-1}])^a$	τ_o (ns) [a,b]	$\lambda_{em[nm]}$ [a]	Φ_F [a]	$K_{nr[ns]}$ [c]	$K_{r[ns]}$ [c]
Benzene	278(6200)	6.83	371,488	0.73	0.04	0.106
Ethyl Acetate	278(16,700)	5.64	371,508	0.68	0.056	0.121
THF	308(19,600)	6.19	508	0.90	0.017	0.145
DCM	250(29,400)	10.62	370,513	0.43	0.054	0.04
Pyridine	317(19,600)	2.90	524	0.95	0.019	0.326
Methanol	252(15,700)	3.83	371	0.37	0.164	0.097

Table 2. Solvatochromic properties of P_5. [a]Measured in CH_2Cl_2 at 25 μM and room temperature. Uncertainty for λ_{abs} and λ_{em}: ± 1 nm. Uncertainty for τ_o ± 0.3 ns. [b]Lifetimes measured using CH_2Cl_2 under an inert atmosphere. Uncertainty for τ_o: ± 0.1 ns. [c]Rates constants of radiative (k_r) and non-radiative (k_{nr}) decay calculated using the formula $K_r = \frac{\Phi F}{\tau o}$ and $K_{nr} = \frac{(1-\Phi F)}{\tau o}$.

Solvatochromic behavior of P_5. The absorption and emission maxima of P_5 exhibited pronounced shifts as a function of solvent polarity (Figs. 4, 5 and Table 2). The absorption maxima shifted significantly as the solvent polarity was increased, implying that the ground state is also affected by the solvent polarity possibly due to a change in the dipole moment of the dye in the ground state[49,50]. A shift of 65 nm was found between methanol to pyridine. Similar shifts were obtained in the case of fluorescence along with the dual emission behaviour.

Previously reported similar compounds[36] were found to show dual emission and solvatochromism having one band, F_1, at around 370 nm that was independent of the solvent but a second band, F_2, at a longer wavelength which was solvent sensitive. Interestingly, both emission bands were found to be solvent responsive for P_5 in specific organic solvents (Fig. 5). For instance, in the case of THF and pyridine, while the F_1 band disappeared, the second emission band (F_2) was observed with maxima at 508 and 524 nm, respectively. Another interesting solvent-dependent feature is the quenching by solvents capable of hydrogen bonding, presumably due to a form of hydrogen-bonded charge transfer[51]. For protic solvents, strong quenching and shorter lifetime are due to the additional interactions that are common for protic solvents. This feature can be utilized to probe the protic solvents as well for the complex biological systems[52].

Although the origin of dual fluorescence is still not clear, there are various hypotheses to explain the phenomenon[53]. Fluorophores with D-A configuration upon absorption of a photon, undergo an internal proton transfer from a donor part of the molecule to an acceptor that results in a relaxed perpendicular conformer which exists in equilibrium with the coplanar conformer. These geometry changes result in dual emission, where a narrow high energy band is the result of local excitation (LE = 370 nm) and a lower energy broader band emerges due to TICT[54]. In the TICT state, the donor part is highly twisted with respect to the acceptor part of the complex resulting in charge separation, increasing the solvent polarity pushes the equilibrium favouring the TICT that potentially accounts for the disappearance of the LE band when using THF and pyridine. It is noteworthy this behaviour was only observed with specific polar solvents having donor atoms, hence complex-solvent interactions need to be considered[55].

The excited-state lifetimes revealed that except in the case of methanol and DCM, higher radiative rates and higher emission efficiency are favoured as can be seen in Table 2. Particularly, solvents with donor atoms exhibited a special effect on the quantum yields (PLQY) as well, as their values reached up to 0.95 for pyridine and 0.90 for

THF. While a very short excited state lifetime confirmed their origin to be TICT. Furthermore, strong quenching and shortening of the lifetime were noticed for typical protic solvents, owing to hydrogen bonding interactions.

Conclusions

A new series of diphenyl boron (III) complexes bearing unsymmetric pyridine-pyrazolate ligands with donor–acceptor (D–A) features has been synthesised and characterized using ^{1}H, ^{13}C NMR and HRMS analysis. The complexes exhibited tunable emission, high luminescence efficiency and large Stokes shift properties depending on the electronic nature of the functional groups on the ligands. The longer Stokes shift along with longer lifetime compared to classical BODIPYs renders them strong candidates for applications as probes requiring a longer life with minimal self-quenching and background scattering. Selected complexes (P_5) displayed dual emission behaviour and interesting solvatochromic behaviour. Owing to the quenching behaviour observed for complexes in H-bonding solvents, this complex could be potentially useful in sensing applications for the detection of a biologically and environmentally interesting analyte. The future investigation includes the modification of synthesised compounds by cleaving –OMe to –OH to tag various antibodies for analysis. Secondly, the –Br functional group provides a potential centre for further modifications and tuning to obtain dyes that can potentially emit in the NIR region.

Experimental

Methods. NMR and HRMS graphs are reported in the supporting information. Where otherwise noted, all chemicals purchased were from a commercial supplier and were used without further purification. The THF solvent used for the synthesis of 1,3-diketones were first dried with a molecular sieve 4 Å and was stored under a nitrogen atmosphere for 72 h before being used. All the reactions were carried out under an inert atmosphere of argon. The progress of the reaction was monitored by TLC analysis. High-resolution mass spectra were recorded with a mass spectrometer (Agilent 6538 Q-TOF with dual ESI source). ^{1}H and ^{13}C NMR spectra were recorded on a Bruker Advance spectrometer [400 MHz (^{1}H) and 100 MHz (^{13}C) in $CDCl_3$ (first de-acidified by passing it through calcium carbonate before testing) and with DMSO. The solvent peaks were referenced according to the literature[56]. UV–visible absorption spectra were recorded on Eppendorf UV–Vis spectrophotometer. The fluorescence spectra were measured on Varian carry fluorescence spectrophotometer. The fluorescence lifetime was determined using Fluoromax-4 fluorimeter (Horiba) in a quartz cuvette (Starna). Excitation was carried out using a 293-nm delta diode (Horiba) in Fluoromax-4C-TCSPC configuration. The diode was pulsed at a 2 MHz repetition rate, the decay was measured until 10,000 counts were reached in the peak channel.

Materials. 2-Picolinic acid (98-98-6), sulphur acid (7664-93-9), sodium bicarbonate (144-55-8), sodium hydride (7646-69-7), 6-methoxy 2-acetonaphthone (3900-45-6), 4-bromo acetophenone (99-90-1), acetophenone (98-86-2), 4-methoxy acetophenone (100-06-1), 4-acetylpyridine (1122-54-9), 2-acetyl anthracene (784-04-3), magnesium sulfate (7487-88-9), hydrazine hydrate (10,217-52-4), triphenyl borane (960-71-4), quinine hemisulfate salt monohydrate (207,671-44-1), sodium chloride (7647-14-5), silica (112,926-00-8), molecular sieves $4A^0$ (20,300), methanol (67-56-1), dichloromethane (75-09-2), tetrahydrofuran (109-99-9), Pyridine (110-86-1), chloroform (67-66-3), ethanol (64-17-5), chloroform-d (865-49-6), DMSO-d_6 (2206-27-1) were purchased from Sigma Aldrich, Australia. Methyl picolinate used for the synthesis of 1,3-diketones was synthesized according to a reported method[57].

Synthesis of 1, 3-diketone. *General procedure.* Sodium hydride (5 equivalent) was suspended in dry THF (40 mL) in an ice bath. To this methyl picolinate (2.5 equivalent), suitable acetophenone (1 equivalent) was added under an atmosphere of argon. The resulting mixture was refluxed overnight under an atmosphere of argon. After cooling the reaction mixture to room temperature, it was poured into ice and neutralized with acetic acid (2 mL). The crude material was extracted with DCM (3 × 30 mL). The combined organic layers were washed with brine (2 × 50 mL), dried over magnesium sulfate, filtered, and evaporated to afford crude material. This was further purified by column chromatography on silica gel with a suitable combination of solvents as eluent.

1-phenyl-3-(pyridine-2-yl) propane-1, 3-dione (B_1). Sodium hydride (50 mg, 20.4 mmol), methyl picolinateA_1 (2.85 g, 20.8 mmol) and acetophenone (1.00 g, 8.3 mmol) was used. The crude material was purified using column chromatography (silica, DCM, *n*-hexane 1:1) to afford $\mathbf{B_1}$ (1.13 g, 60%) as a yellow solid. ^{1}H NMR (400 MHz, $CDCl_3$) 7.44–7.58 (m, 5H, ArH), 7.83–7.88 (m, 1H, ArH), 8.06–8.09 (m, 2H, ArH), 8.15–8.17 (m, 1H, ArH), 8.70–8.72 (m, 1H, ArH), 16.47 (s, 1H, OH enolic) ppm. ^{13}C NMR (100 MHz, $CDCl_3$) 93.69, 122.26, 126.48, 127.57, 127.62, 128.77, 128.82, 132.78, 135.45, 137.17, 149.41, 152.68, 183.64, 186.42 ppm. HRMS (ESI, TOF) m/z calcd for $C_{14}H_{12}NO_2$, 226.0868; found 226.08606, the data are in agreement with the reported literature[58].

1-(4-bromophenyl)-3-(pyridine-2-yl) propane-1, 3-dione (B_2). Sodium hydride (30 mg, 20.4 mmol), methyl picolinateA_1 (1.72 g, 12.6 mmol) and 4-bromo acetophenone (1.00 g, 5.0 mmol) was used. The crude material was purified using column chromatography (silica gel, ethyl acetate, *n*-hexane 2:8) to afford $\mathbf{B_2}$ (98 mg, 64%) as a yellow solid. ^{1}H NMR (400 MHz, $CDCl_3$) 7.44–7.51 (m, 1H, ArH), 7.55 (s, 1H, CH, enolic), 7.63 (d, 2H, J = 8.52 Hz, ArH), 7.85–7.95 (m, 3H, ArH), 8.18 (d, 1H, J = 7.96 Hz, ArH), 16.35 (s, 1H, enolic, OH) ppm. ^{13} C NMR (100 MHz, $CDCl_3$) 93.75, 122.34, 126.64, 127.62, 127.69, 128.77, 129.08, 132.07, 132.15, 134.33, 137.22, 149.43, 152.46, 184.14, 185.05 ppm. HRMS (ESI, TOF) m/z calcd for $C_{14}H_{12}NO_2$ Br, 303.99731; found 303.99662.

1-(4-methoxyphenyl)-3-(pyridine-2-yl) propane-1, 3-dione (B_3). Sodium hydride (40 mg, 16.7 mmol), methyl picolinateA_1 (2.28 g, 16.7 mmol) and 4-methoxy acetophenone (1.00 g, 6.67 mmol) were used. The crude material was purified using column chromatography (silica gel, ethyl acetate, *n*-hexane 3:7) to afford **B_3** (1.59 g, 94%)[59] as a bright yellow solid. ^{1}H NMR (400 MHz, $CDCl_3$) 3.89 (s, 3H, OCH_3), 6.96–7.00 (m, 3H, ArH), 7.23–7.27 (m, 1H, ArH), 7.74–7.81 (m, 4H, ArH), 8.68 (d, 1H, *J* = 4.9 Hz, ArH),16.63 (s, 1H, –OH enolic) ppm. ^{13}C NMR (100 MHz, $CDCl_3$) 55.54, 93.60, 105.89, 119.82, 122.22, 124.31, 126.37, 127.26, 128.25, 128.87, 130.64, 131.20, 137.18, 137.29, 149.39, 152.78, 159.77, 182.78, 186.91 ppm. HRMS (ESI, TOF) m/z calcd for $C_{15}H_{14}NO_3$, 256.09737; found 256.09653.

1-(pyridine-2-yl)-3-(pyridine-4-yl) propane-1, 3-dione (B_4). Sodium hydride (49 mg, 20.7 mmol), methyl picolinateA_1 (86 mg, 6.3 mmol) and 4-acetyl pyridine (1.00 g, 8.3 mmol) were used. The crude material was purified using column chromatography (silica gel, ethyl acetate, *n*-hexane 1:1) to afford **B_5** (55 mg, 29%) as bright yellow solid[60] . ^{1}H NMR (400 MHz, $CDCl_3$) 7.41–7.44 (m, 2H, ArH), 7.80–7.88 (2H, ArH), 8.14 (d, 3H, *J* = 7.9 Hz, ArH), 8.73–8.74 (m, 2H, ArH), 15.94 (s, 1H, enolic –OH) ppm. ^{13}C NMR (100 MHz, $CDCl_3$) 94.67, 122.07, 122.24, 126.49, 127.30, 136.99, 137.03, 149.01, 149.63, 152.56, 184.56, 197.06 ppm. HRMS (ESI, TOF) m/z calcd for $C_{13}H_{11}N_2O_2$, 227.08205; found 227.08128.

1-(6-methoxy naphthalene-2-yl)-3-(pyridine-2-yl) propane-1, 3-dione (B_5). Sodium hydride (15 mg, 6.3 mmol), methyl picolinateA_1 (86 mg, 6.3 mmol) and 6-methoxy 2-acetonaphthone (50 mg, 2.5 mmol) were used. The crude material was purified using column chromatography (silica gel, ethyl acetate, *n*-hexane 1:9) to afford **B_4** (67 mg 93%) as bright yellow solid. ^{1}H NMR (400 MHz, $CDCl_3$) 3.88 (s, 3H, OCH_3), 6.95–6.99 (m, 2H, ArH), 7.40–7.44 (m, 1H, ArH), 7.50 (s, 1H, C=CH), 7.85 (t,d 1H, *J* = 7.8 Hz, 1.8 Hz, ArH), 8.04–8.07 (m, 1H, ArH), 8.14 (d, 1H, *J* = 7.9 Hz, ArH), 8.69–8.71 (m, 1H, ArH), 16.62 (s, 1H, enolic –OH) ppm. ^{13}C NMR (100 MHz, $CDCl_3$) 55.43, 93.49, 105.79, 119.70, 122.11, 124.21, 126.24, 127.15, 128.15, 128.76, 130.55, 131.09, 137.07, 137.17, 149.27, 152.69, 159.66, 182.66, 186.81 ppm. HRMS (ESI, TOF) m/z calcd for $C_{19}H_{16}NO_3$, 306.11302; found 306.11220.

1-(anthracene-2-yl)-3-(pyridine-2-yl) propane-1, 3-dione (B_6). Sodium hydride (14 mg, 5.7 mmol), methyl picolinateA_1 (78 mg, 5.7 mmol) and 3-acetyl anthracene (50 mg, 2.3 mmol) were used. The crude material was purified using column chromatography (silica gel, ethyl acetate, *n*-hexane 1:9) to afford **B_6** (55 mg, 74%). as a dull yellow solid.[1,61] ^{1}H NMR (400 MHz, $CDCl_3$) 7.45–7.48 (m, 1H, ArH), 7.63–7.81 (m, 4H, ArH, C=CH), 7.84 (d, 1H, *J* = 8.9 Hz, ArH), 7.88–7.93 (m, 2H, ArH), 7.96 (d, 1H, *J* = 8.4 Hz, ArH), 8.20–8.25 (m, 2H, ArH), 8.76–8.78 (m, 1H, ArH), 8.85 (d, 1H, *J* = 8.2 Hz, ArH), 9.43 (s, 1H, ArH), 16.70 (s, 1H, enolic –OH) ppm. ^{13}C NMR (100 MHz, $CDCl_3$) 122.35, 122.98, 123.10, 123.41, 124.87, 126.48, 126.53, 127.31, 127.38, 128.86, 128.92, 129.04, 129.64, 130.15, 132.34, 133.15, 134.98, 137.23, 149.44, 152.79, 184.00, 186.33 ppm. HRMS (ESI, TOF) m/z calcd for $C_{22}H_{16}NO_2$, 326.1181; found 326.11734.

Synthesis of Pyridine-Pyrazole ligands. *General procedure.* Suitable 1, 3- diketone (1 equivalent) and hydrazine hydrate (3 equivalent) were dissolved in ethanol (30 mL) and heated to reflux overnight. The solvent was evaporated to dryness under reduced pressure to afford the respective pyridine-pyrazole ligands. The crude material was used without further purification.

2-(3-phenyl-1H-pyrazol-5-yl) pyridine (C_1). Starting with B_1 (50 mg, 2.2 mmol) and hydrazine hydrate (28 mg, 5.6 mmol), the crude C_1 was obtained as a colourless solid (45 mg, 90%), which was used further without purification. ^{1}H NMR (400 MHz, $CDCl_3$) 7.11–7.13 (m, 1H, ArH), 7.26–7.33 (m, 1H, ArH), 7.35 (d, 1H, *J* = 6.9 Hz, ArH), 7.44 (t, 2H, *J* = 7.2 Hz, ArH), 7.79–7.86 (m, 4H, ArH), 8.66 (d, 1H, J = 4.9 Hz, ArH) ppm. ^{13}C NMR (100 MHz, $CDCl_3$) 100. 68, 120.37, 123.16, 125.82, 127.84, 128.24, 128.30, 128.60, 128.91, 132.53, 137.59, 144.64, 148.55, 149.18, 151.61 ppm. HRMS (ESI, TOF) m/z calcd for $C_{14}H_{12}N_3$, 222.10312; found 222.10246.

2-(3-(4-bromophenyl)-1H-pyrazol-5-yl) pyridine (C_2). Starting with B_2 (40 mg, 1.3 mmol) and hydrazine hydrate (1.7 mg, 3.3 mmol), the crude C_2 was obtained as a colourless solid (37 mg, 92%), which was used without further purification. ^{1}H NMR (400 MHz, DMSO) 7.30–7.99 (m, 8H, ArH), 8.60 (s, 1H, ArH), 13.66, 13.56 (s, 1H, N= NH) ppm. ^{13}C NMR (100 MHz, DMSO-d_6) 100.78, 100.99, 101.18, 119.20, 119.99, 120.46, 121.24, 122.63, 123.07, 125.07, 127.07, 129.00, 131.57, 131.93, 132.76, 136.74, 137.36, 142.29, 143.31, 147.83, 149.17, 149.41, 150.12, 151.95, 152.32 ppm. HRMS (ESI, TOF) m/z calcd for $C_{14}H_{11}BrN_3$, 300.01363; found 300.01290.

2-(3-(4-methoxyphenyl)-1H-pyrazol-5-yl) pyridine (C_3). Starting with B_3 (1.00 g, 3.9 mmol) and hydrazine hydrate (49 mg, 9.8 mmol), the crude C_3 was obtained as a pink solid (98 mg, 100%), which was used without further purification. ^{1}H NMR (400 MHz, $CDCl_3$) 3.85 (s, 3H, OCH_3), 6.96–7.00 (m, 3H, ArH), 7.23–7.27 (m, 1H, ArH), 7.74–7.81 (m, 4H, ArH), 8.68 (d, 1H, *J* = 4.9 Hz, ArH), 11.55 (s, 1H, NH) ppm. ^{13}C NMR (100 MHz, $CDCl_3$) 55.64, 93.02, 114.09, 122.11, 126.24, 128.25, 129.87, 137.16, 149.38, 152.76, 163.59, 181.71, 187.12 ppm. HRMS (ESI, TOF) m/z calcd for $C_{15}H_{14}N_3O$, 252.11369; found 252.11289.

2-(3-(pyridin-4-yl)-1H-pyrazol-5-yl) pyridine (C_4). Starting with B_4 (30 mg, 1.3 mmol) and hydrazine hydrate (16 mg, 3.3 mmol), the crude C_4 was obtained as a yellowish solid. (27 mg, 92%), which was used without further purification. ^{1}H NMR (400 MHz, $CDCl_3$) 7.24–7.27 (m, 3H, ArH), 7.41 (s, 1H, CH), 7.74–7.80 (m, 2H, ArH), 7.91 (d, 2H, *J* = 7.9 Hz, ArH), 8.66 (d, 2H, *J* = 4.4 Hz) ppm. ^{13}C NMR (100 MHz, $CDCl_3$) 101.97, 120.41, 121.94,

123.01, 137.21, 137.42, 148.21, 149.44, 150.13 ppm. HRMS (ESI, TOF) m/z calcd for $C_{13}H_{11}N_4$, 223.09837; found 223.09772.

2-(3-(6-methoxynaphthalen-2-yl)-1H-pyrazol-5-yl) pyridine (C_5). Starting with B_5 (50 mg, 1.73 mmol) and hydrazine hydrate (21 mg, 4.3 mmol), the crude C_5 was obtained as a yellowish solid (46 mg, 94%), which was used without further purification. ^{1}H NMR (400 MHz, DMSO-d_6) 3.89 (s, 3H, OCH_3), 7.19 (d, 1H, J = 8.3 Hz, ArH), 7.35 (s, 3H, ArH), 7.85–7.98 (m, 5H, ArH), 8.30 (s, 1H, CH), 8.63 (s, 1H, ArH), 13.56 (s, 1H, NH) ppm. ^{13}C NMR (100 MHz, DMSO-d_6) 55.17, 55.22, 100.74, 100.81, 105.97, 118.85, 119.17, 119.32, 119.94, 122.52, 122.97, 123.35, 123.67, 123.87, 124.14, 124.37, 126.99, 127.45, 129.39, 128.57, 128.83, 129.47, 129.53, 133.75, 133.90, 136.69, 137.35, 143.15, 143.60, 148.02, 149.16, 149.41, 151.35, 152.18, 152.23 ppm. HRMS (ESI, TOF) m/z calcd for $C_{19}H_{16}N_3O$, 302.12934; found 302.12852.

2-(3-(anthracen-2-yl)-1H-pyrazol-5-yl) pyridine (C_6). Starting with B_6 (40 mg, 1.2 mmol) and hydrazine hydrate (15 mg, 3.0 mmol), the crude C_6 was obtained as a yellow solid (39 mg, 99%) which was used without further purification. ^{1}H NMR (400 MHz, DMSO-d_6) 7.30–8.24 (m, 11H, ArH), 8.65 (s, 1H, ArH), 9.03 (dd, 1H, J = 11.4 Hz, 7.30 Hz, ArH), 9.3 (s, 1H, apparent doublet due to H-bonding), 13.71 (s, 1H, N=NH), 13.76 (s, 1H, HN=N) ppm. ^{13}C NMR (100 MHz, DMSO) 91.32, 96.06, 98.69, 101.27, 101.59, 102.01, 105.41, 106.06, 114.59, 118.95, 119.27, 119.99, 122.63, 123.05, 123.30, 123.98, 124.37, 126.58, 126.89, 127.11, 127.35, 128.54, 128.92, 129.26, 129.81, 130.04, 131.02, 131.15, 131.56, 131.88, 136.77, 137.40, 143.33, 143.60, 148.07, 149.21, 149.44 ppm. HRMS (ESI, TOF) m/z calcd for $C_{22}H_{16}N_3$, 322.13442; found 322.13362.

Synthesis of pyridine-pyrazole boron complexes. *General procedure.* Pyridine pyrazole ligand (1 equivalent) and triphenyl borane (1 equivalent) were dissolved in toluene (20 mL) and the resulting mixture was heated to reflux overnight under an atmosphere of argon. After the completion of the reaction was confirmed by TLC, the solvent was evaporated under reduced pressure. The residue was dissolved in DCM (40 mL) and the organic layer was washed with brine (50 mL), dried over magnesium sulfate, filtered and evaporated to obtain white and yellow material. The residue was purified using column chromatography on silica gel and a suitable combination of organic solvents.

2-(5-phenyl-1H-pyrazol-3-yl) pyridine Boron Complex (P_1). Starting with C_1 (7 mg, 0.3 mmol) and triphenyl borane (8 mg, 0.3 mmol) in toluene, the crude material was collected and purified using column chromatography (silica, ethyl acetate: *n*-hexane 1:1) to afford P_1 as a white solid (108 mg, 34%). ^{1}H NMR (400 MHz, $CDCl_3$) 7.02 (s, 1H, ArH), 7.20–7.30 (m, 7H, ArH), 7.34–7.40 (m, 7H, ArH), 7.80 (d, t, 1H, J = 8.1 Hz, 1.0 Hz, ArH), 7.92–7.95 (m, 2H, ArH), 8.04 (d, t, 1H, J = 7.8 Hz, 1.1 Hz, ArH), 7.80 (d,t, 1H, J = 5.8 Hz, 1.0 Hz, ArH) ppm. ^{13}C NMR (100 MHz, $CDCl_3$) 97.52, 118.51, 121.85, 125.78, 126.07, 127.18, 127.52, 127.84, 128.07, 128.61, 128.92, 132.96, 134.40, 134.85, 141.59, 141.87, 143.28, 147.69, 157.56 ppm. HRMS (ESI, TOF) m/z calcd for $C_{26}H_{20}BN_3B$, 385.18649; found 386.18240.

2-(3-(4-bromophenyl)-1H-pyrazol-5-yl) pyridine Boron Complex (P_2). Starting with C_2 (20 mg, 0.7 mmol) and triphenyl borane (16 mg, 0.7 mmol) in toluene, the crude material was collected and purified using column chromatography (silica, ethyl acetate: *n*-hexane 1:1) to afford P_2 as a white solid (0.96 mg, 46%). ^{1}H NMR (400 MHz, DMSO-d_6) 7.14–7.26 (m, 10H, ArH), 7.42 (s, 1H, C=CH), 7.59–7.61 (m, 2H, ArH), 7.68–7.72 (m, 1H, ArH), 7.82–7.85 (m, 2H, ArH), 8.25 (d, 1H, J = 8.0 Hz, ArH), 8.42 (t, d, 1H, J = 7.9 Hz, 1.4 Hz, ArH), 8.88 (d, 1H, J = 5.8 Hz, ArH) ppm. ^{3}C NMR (100 MHz, DMSO-d_6) 98.01, 119.24, 120.24, 123.59, 125.28, 126.69, 127.07, 127.42, 128.18, 128.87, 131.58, 132.26, 133.16, 137.31, 142.02, 143.67, 143.92, 145.76, 154.71 ppm. HRMS (ESI, TOF) m/z calcd for $C_{26}H_{20}BBrN_3$, 464.0934; found 464.0941.

2-(3-(4-methoxyphenyl)-1H-pyrazol-5-yl) pyridine Boron Complex (P_3). Starting with C_3 (30 mg, 1.2 mmol) and triphenyl borane (29 mg, 1.2 mmol) in toluene, the crude material was collected and purified using column chromatography (silica, ethyl acetate: *n*-hexane 1:1) to afford P_3 as a light-yellow solid (29 mg, 59%). ^{1}H NMR (400 MHz, $CDCl_3$) 3.82 (s, 3H, OCH_3), 6.92–7.01 (m, 3H, ArH), 7.21–7.28 (m, 7H, ArH), 7.31–7.37 (m, 4H, ArH), 7.41–7.48 (m, 1H, ArH), 7.91–7.97 (m, 3H, ArH), 8.10–8.14 (m, 1H, ArH), 8.51 (d, 1H, J = 5.6 Hz, ArH) ppm. ^{13}C NMR (100 MHz, $CDCl_3$) 29.69, 55.30, 96.86, 113.70, 113.90, 118.53, 121.92, 127.09, 127.34, 127.70, 127.89, 128.72, 130.49, 131.02, 132.71, 132.84, 134.69, 141.44, 141.83, 143.15, 147.22, 156.90, 159.33 ppm. HRMS (ESI, TOF) m/z calcd for $C_{27}H_{23}BN_3O$, 416.1934; found 416.1933.

2-(3-(pyridin-4-yl)-1H-pyrazol-5-yl) pyridine Boron Complex (P_4). Starting with C_4 (15 mg, 0.7 mmol) and triphenyl borane (16 mg, 0.7 mmol) in toluene, the crude material was collected and purified using column chromatography (silica, ethyl acetate: *n*-hexane 1:1) to afford P_4 as an off white solid (052 mg, 19%). ^{1}H NMR (400 MHz, $CDCl_3$) 7.13–7.19 (m, 1H, ArH), 7.23–7.29 (m, 6H, ArH), 7.33–7.39 (m, 5H, ArH), 7.45 (s, 1H, C=CH), 7.68 (t, 1H, J = 7.7 Hz, ArH), 7.84 (d, 1H, J = 8.1 Hz, ArH), 8.05 (t, 1H, J = 7.7 Hz, ArH), 8.20 (d, 1H, J = 8.1 Hz, ArH), 8.50 (d, 1H, J = 5.9 Hz, ArH), 8.61 (d, 1H, J = 4.8 Hz, ArH) ppm. ^{13}C NMR (100 MHz, $CDCl_3$) 99.77, 119.09, 121.16, 122. 44, 122.68, 127.60, 128.21, 133.30, 136.97, 142.11, 142.36, 143.61, 147.98, 149.51, 153.42, 158.25 ppm. HRMS (ESI, TOF) m/z calcd for $C_{25}H_{20}BN_4$, 387.1781; found 387.1781.

2-(6-Methoxynaphthelene) 5-(2-pyridyl) pyrazolate boron Complex (P_5). Starting with C_5 (20 mg, 0.7 mmol) and triphenyl borane (16 mg, 0.7 mmol) in toluene, the crude material was collected and purified using column

chromatography (silica, ethyl acetate: *n*-Hexane 1:1) to afford P_5 as an off white solid (17 mg, 54%). ^{1}H NMR (400 MHz, $CDCl_3$) 3.92 (s, 3H, -OCH_3), 7.11–7.14 (m, 3H, ArH), 7.22–7.29 (m, 7H, ArH), 7.34–7.39 (m, 5H, ArH), 7.75 (d, 1H, *J* = 8.5 Hz, ArH), 7.78 (d, 1H, *J* = 4.8 Hz, ArH), 7.82 (tt, 1H, *J* = 8.1, 0.9 Hz, ArH), 8.01–8.07 (m, 2H, ArH), 8.31 (s, 1H, ArH), 8.51–8.53 (m, 1H, ArH) ppm. ^{13}C NMR (100 MHz, $CDCl_3$) 53.44, 55.30, 97.40, 105.78, 118.39, 118.82, 121.73, 124.17, 125.16, 126.88, 127.09, 127.75, 127.94, 129.12, 129.62, 129.72, 132.88, 134.09141.54, 141.76, 143.17, 147.56, 157.53, 157.59 ppm. HRMS (ESI, TOF) m/z calcd for $C_{31}H_{25}BN_3O$, 466.2091; found 466.2099.

2-(5-(anthracen-2-yl)-1H-pyrazol-3-yl) pyridine (P_6). Starting with C_6 (20 mg, 0.6 mmol) and triphenyl borane (15 mg, 0.6 mmol) in toluene, the crude material was collected and purified using column chromatography (silica gel, ethyl acetate: *n*-hexane 1:1) to afford P_6 as a yellow solid. (27 mg, 92%). ^{1}H NMR (400 MHz, DMSO-d_6) 7.18–7.31 (m, 10H, ArH), 7.66 (t, 1H, *J* = 6.9 Hz, ArH), 7.69–7.73 (m 2H, ArH), 7.81 (d, 1H, *J* = 8.9 Hz, ArH), 7.85 (d, 1H, *J* = 8.9 Hz, ArH), 7.98 (d, 1H, *J* = 8.0 Hz, ArH), 8.02 (d, 1H, *J* = 8.4 Hz, ArH), 8.23 (d, 1H, *J* = 8.4 Hz, ArH), 8.26 (d, 1H, *J* = 8.0 Hz, ArH), 8.45 (t, 1H, *J* = 7.9 Hz, ArH), 8.90 (d, 1H, *J* = 5.7 Hz, ArH), 8.94 (d, 1H, *J* = 8.3 Hz, ArH), 9.24 (s, 1H, ArH) ppm. ^{13}C NMR (100 MHz, DMSO-d_6) 99.04, 119.08. 119.62, 123.51, 124.62, 124.78, 127.02, 127.11, 127.22, 127.32, 127.39, 127.96, 129.03, 129.43, 130.24, 130.47, 131.41, 132.36, 132.88, 142.59, 144.24, 144.46, 146.41 ppm. HRMS (ESI, TOF) m/z calcd for $C_{34}H_{25}BN_3$, 485.2178; found 486.21337.

Data availability

All data generated or analysed during this study are included in this published article and its supplementary information file. The data is also available through a request from the corresponding author.

Received: 9 August 2022; Accepted: 19 September 2022
Published online: 01 October 2022

References

1. Whittell, G. R., Hager, M. D., Schubert, U. S. & Manners, I. Functional soft materials from metallopolymers and metallosupramolecular polymers. *Nat. Mater.* **10**(3), 176–188 (2011).
2. Kumaresan, D., Thummel, R. P., Bura, T., Ulrich, G. & Ziessel, R. Color tuning in new metal-free organic sensitizers (Bodipys) for dye-sensitized solar cells. *Chem. Eur. J.* **15**(26), 6335–6339 (2009).
3. Baumes, J. M. *et al.* Storable, thermally activated, near-infrared chemiluminescent dyes and dye-stained microparticles for optical imaging. *Nat. Chem.* **2**(12), 1025–1030 (2010).
4. Gonçalves, M. S. T. Fluorescent labeling of biomolecules with organic probes. *Chem. Rev.* **109**(1), 190–212 (2009).
5. Araneda, J. F., Piers, W. E., Heyne, B., Parvez, M. & McDonald, R. High stokes shift anilido-pyridine boron difluoride dyes. *Angew. Chem. Int. Ed* **50**(51), 12214–12217 (2011).
6. Frath, D., Massue, J., Ulrich, G. & Ziessel, R. Luminescent materials: Locking π-conjugated and heterocyclic ligands with Boron(III). *Angew. Chem.* **53**(9), 2290–2310 (2014).
7. Li, D., Zhang, H. & Wang, Y. Four-coordinate organoboron compounds for organic light-emitting diodes (OLEDs). *Chem. Soc. Rev.* **42**(21), 8416–8433 (2013).
8. Molander, G. A. & Ham, J. Synthesis of functionalized organotrifluoroborates via halomethyltrifluoroborates. *Org. Lett.* **8**(10), 2031–2034 (2006).
9. Loudet, A. & Burgess, K. BODIPY dyes and their derivatives: Syntheses and spectroscopic properties. *Chem. Rev.* **107**(11), 4891–4932 (2007).
10. Suzuki, S., Kozaki, M., Nozaki, K. & Okada, K. Recent progress in controlling photophysical processes of donor–acceptor arrays involving perylene diimides and boron-dipyrromethenes. *J. Photochem. Photobiol.* **12**(4), 269–292 (2011).
11. Hong, X. *et al.* Silylated BODIPY dyes and their use in dye-encapsulated silica nanoparticles with switchable emitting wavelengths for cellular imaging. *Analyst* **137**(18), 4140–4149 (2012).
12. Mizusawa, K., Takaoka, Y. & Hamachi, I. Specific cell surface protein imaging by extended self-assembling fluorescent turn-on nanoprobes. *J. Am. Chem. Soc.* **134**(32), 13386–13395 (2012).
13. Kamkaew, A. *et al.* BODIPY dyes in photodynamic therapy. *Chem. Soc. Rev.* **42**(1), 77–88 (2013).
14. Lovell, J. F., Liu, T. W. B., Chen, J. & Zheng, G. Activatable photosensitizers for imaging and therapy. *Chem. Rev.* **110**(5), 2839–2857 (2010).
15. Yuan, L., Lin, W., Zheng, K., He, L. & Huang, W. Far-red to near infrared analyte-responsive fluorescent probes based on organic fluorophore platforms for fluorescence imaging. *Chem. Soc. Rev.* **42**(2), 622–661 (2013).
16. Kim, H. N., Ren, W. X., Kim, J. S. & Yoon, J. Fluorescent and colorimetric sensors for detection of lead, cadmium, and mercury ions. *Chem. Soc. Rev.* **41**(8), 3210–3244 (2012).
17. Erten-Ela, S. *et al.* A Panchromatic boradiazaindacene (BODIPY) sensitizer for dye-sensitized solar cells. *Org. Lett.* **10**(15), 3299–3302 (2008).
18. Ooyama, Y., Hagiwara, Y., Mizumo, T., Harima, Y. & Ohshita, J. The case for organic photovoltaics. *RSC Adv.* **3**(39), 18099–18106 (2013).
19. Yang, R. & Sun, M. Bilayer borophene synthesized on Ag(111) film: Physical mechanism and applications for optical sensor and thermoelectric devices. *Mater. Today Phys.* **23**, 100652 (2022).
20. Burghart, A. *et al.* Energy transfer cassettes based on BODIPY® dyes. *ChemComm* **22**, 2203–2204 (2000).
21. Zhou, Y., Xiao, Y., Chi, S. & Qian, X. Isomeric boron–fluorine complexes with donor–acceptor architecture: Strong solid/liquid fluorescence and large stokes shift. *Org. Lett.* **10**(4), 633–636 (2008).
22. Hu, R. *et al.* Synthesis, solvatochromism, aggregation-induced emission and cell imaging of tetraphenylethene-containing BODIPY derivatives with large Stokes shifts. *Chem. Commun.* **48**(81), 10099–10101 (2012).
23. Divakar, S. *et al.* Iminoenamine based novel androgen receptor antagonist exhibited anti-prostate cancer activity in androgen independent prostate cancer cells through inhibition of AKT pathway. *Chem.-Biol. Interact.* **275**, 22–34 (2017).
24. Tian, C., Chen, Y., Yan, P., Sun, M. & Quan, J. Physical mechanisms of photoinduced charge transfer in neutral and charged donor–acceptor systems. *RSC Adv.* **11**(60), 38302–38306 (2021).
25. Zhu, S. & Sun, M. Photoinduced charge transfer in two-photon absorption. *Res. Opt.* **4**, 100099 (2021).
26. Mu, X., Wang, J. & Sun, M. Visualization of photoinduced charge transfer and electron-hole coherence in two-photon absorption. *Phys. Chem. C.* **123**(23), 14132–14143 (2019).

27. Shirota, Y., Kinoshita, M., Noda, T., Okumoto, K. & Ohara, T. A novel class of emitting amorphous molecular materials as bipolar radical formants: 2-{4-[Bis(4-methylphenyl)amino]phenyl}- 5-(dimesitylboryl)thiophene and 2-{4-[Bis(9,9-dimethylfluorenyl) amino]phenyl}- 5-(dimesitylboryl)thiophene. *J. Am. Chem. Soc.* **122**(44), 11021–11022 (2000).
28. Hu, R. *et al.* Synthesis, solvatochromism, aggregation-induced emission and cell imaging of tetraphenylethene-containing BODIPY derivatives with large Stokes shifts. *Chem. Commun.* **48**(81), 10099–10101 (2012).
29. Chen, Y., Cheng, Y. & Sun, M. Nonlinear plexcitons: excitons coupled with plasmons in two-photon absorption. *Nanoscale* **14**(19), 7269–7279 (2022).
30. Chen, Y., Cheng, Y. & Sun, M. Physical mechanisms on plasmon-enhanced organic solar cells. *J. Phys. Chem* **125**(38), 21301–21309 (2021).
31. Ren, X. *et al.* Red-emitting boron difluoride complexes with a mega-large Stokes shift and unexpectedly high fluorescence quantum yield. *ChemComm* **56**(14), 2159–2162 (2020).
32. Lugovik, K. I. *et al.* Fluorescent boron complexes based on new *N*, O-chelates as promising candidates for flow cytometry. *Org. Biomol. Chem.* **16**(28), 5150–5162 (2018).
33. Bukowska, P., Piechowska, J. & Loska, R. Azine-imidazole *aza*-BODIPY analogues with large Stokes shift. *Dyes Pigm.* **137**, 312–321 (2017).
34. Liddle, B. J. *et al.* BORAZANs: Tunable fluorophores based on 2-(pyrazolyl) aniline chelates of diphenylboron. *J. Org. Chem.* **72**(15), 5637–5646 (2007).
35. Reilly, D. T., Kim, S. H., Katzenellenbogen, J. A. & Schroeder, C. M. Fluorescent nanoconjugate derivatives with enhanced photostability for single molecule imaging. *Anal. Chem.* **87**(21), 11048–11057 (2015).
36. Cheng, C. *et al.* Syntheses and remarkable photophysical properties of 5-(2-pyridyl) pyrazolate boron complexes; Photoinduced electron transfer. *Chem. Commun.* **20**, 2628–2629 (2003).
37. Satake, A. & Nakata, T. Novel η^3-allylpalladium–pyridinylpyrazole complex: Synthesis, reactivity, and catalytic activity for cyclopropanation of ketene silyl acetal with allylic acetates. *J. Am. Chem. Soc.* **120**(40), 10391–10396 (1998).
38. Zheng, W., Pan, X. M., Cui, L. L., Su, Z. M. & Wang, R. S. Theoretical studies on the structures and absorption spectra of –Ph and *t*-Bu substituted 5-(2-pyridyl) pyrazolate boron complexes. *J. Mol. Struct. THEOCHEM* **809**(1), 39–43 (2007).
39. Williams, D. B. G. & Lawton, M. Drying of organic solvents: Quantitative evaluation of the efficiency of several desiccants. *J. Org. Chem.* **75**(24), 8351–8354 (2010).
40. Javaid, R. *et al.* Design and synthesis of boron complexes as new Raman reporter molecules for sensitive SERS nanotags. *J. Raman Spectrosc.* **51**(12), 2408–2415 (2020).
41. Jones, R. N. The ultraviolet absorption spectra of anthracene derivatives. *Chem. Rev.* **41**(2), 353–371 (1947).
42. Hughes, E. B., Jellinek, H. H. G. & Ambrose, B. A. Pyridine. Ultraviolet absorption spectrum and dissociation constant. *J. Phys. Chem.* **53**(3), 410–414 (1949).
43. Brooker, L. G. S., White, F. L., Sprague, R. H., Dent, S. G. & Van Zandt, G. Anomalous nitration reactions. *Chem. Rev.* **41**(2), 325–351 (1947).
44. Longuet-Higgins, H. C. On the non-orthogonality problem connected with the use of atomic wave functions in the theory of molecules and crystals. *J. Chem. Phys* **18**(3), 265–274 (1950).
45. Brunings, K. J. & Corwin, A. H. Color and constitution. V.[1]The absorption of unsymmetrical cyanines resonance as a basis for a classification of dyes. *J. Am. Chem. Soc.* **64**(3), 593–600 (1942).
46. Kee, L. *et al.* Structural Control Of The Photodynamics Of Boron−Dipyrrin Complexes. *J. Phys. Chem. B* **109**(43), 20433–20443 (2005).
47. Yang, L. *et al.* Asymmetric anthracene-fused BODIPY dye with large Stokes shift: Synthesis, photophysical properties and bioimaging. *Dyes Pigm.* **126**, 232–238 (2016).
48. Ren, T.-B. *et al.* A general method to increase stokes shift by introducing alternating Vibronic structures. *J. Am. Chem. Soc.* **140**(24), 7716–7722 (2018).
49. Acemioğlu, B., Arık, M., Efeoğlu, H. & Onganer, Y. Solvent effect on the ground and excited state dipole moments of fluorescein. *J. Mol. Strcut. (Theochem)* **548**(1–3), 165–171 (2001).
50. Moran, A. M., Delbecque, C. & Kelley, A. M. Solvent effects on ground and excited electronic state structures of the push-pull chromophore Julolidinyl-*n*-*N*, N'-diethylthiobarbituric Acid. *J. Phys. Chem. A* **105**(45), 10208–10219 (2001).
51. Kwok, W.-M. *et al.* Direct observation of a hydrogen-bonded charge-transfer state of 4-dimethylaminobenzonitrile in methanol by time-resolved IR spectroscopy. *Angew. Chem. Int. Ed.* **42**(16), 1826–1830 (2003).
52. Valeur, B. & Berberan-Santos, M. N. *Molecular Fluorescence: Principles and Applications* (John Wiley & Sons, Hoboken, 2012).
53. Kubota, Y., Sakuma, Y., Funabiki, K. & Matsui, M. Solvatochromic fluorescence properties of pyrazine-boron complex bearing a β-iminoenolate ligand. *J. Phys. Chem. A* **118**(38), 8717–8729 (2014).
54. Sasaki, S., Drummen, G. P. C. & Konishi, G. Recent advances in twisted intramolecular charge transfer (TICT) fluorescence and related phenomena in materials chemistry. *J. Mater. Chem. C* **4**(14), 2731–2743 (2016).
55. Qin, W. *et al.* Ratiometric, fluorescent BODIPY dye with aza crown ether functionality: synthesis, solvatochromism, and metal ion complex formation. *J. Phys. Chem. A* **112**(27), 6104–6114 (2008).
56. Fulmer, G. R. *et al.* NMR chemical shifts of trace impurities: Common laboratory solvents, organics, and gases in deuterated solvents relevant to the organometallic chemist. *Organometallics* **29**(9), 2176–2179 (2010).
57. Mamane, V., Aubert, E. & Fort, Y. The Methyl group as a source of structural diversity in heterocyclic chemistry: Side chain functionalization of picolines and related heterocycles. *J. Org. Chem.* **72**(19), 7294–7300 (2007).
58. Dudek, M. *et al.* Interaction of Copper(II) with Ditopic Pyridyl-β-diketone Ligands: Dimeric, framework, and metallogel structures. *Cryst. Growth Des.* **11**(5), 1697–1704 (2011).
59. Soria, L. *et al.* Coordination behaviour of new dipyridylpyrazole ligands towards ZnCl2 and PdCl2 fragments. Crystalline structural characterization and multinuclear NMR studies as evidence of linkage and conformational isomers. *RSC Adv.* **4**(18), 9383–9394 (2014).
60. Ferles, M., Liboska, R. & Trska, P. Asymmetric syntheses of (+)-diltiazem hydrochloride. *Collect. Czech. Chem. Commun.* **55**(5), 1228–1233 (1990).
61. Schowtka, B., Müller, C. I., Görls, H., Westerhausen, M. Synthesis, structures, and spectroscopic properties of 3-Aryl-5-(2-pyridyl) pyrazole.

Acknowledgements

We thank Macquarie University Sydney Australia to support this research through the *i*MQRES scholarship and the Department of Molecular Sciences at Macquarie University for providing facilities to carry out this research. We would also like to thank Dr. Alex Macmillan (Lowy cancer centre UNSW Kensington) for fluorescence lifetime studies.

Author contributions

R.J. designed and carried out the synthesis & charcterization N.S. and M.K. contributed to it. A.R. and R.J. did the photo-physical studies. M.A. helped with the manuscript.

Competing interests

The authors declare no competing interests.

Additional information

Supplementary Information The online version contains supplementary material available at https://doi.org/10.1038/s41598-022-20796-2.

Correspondence and requests for materials should be addressed to R.J.

Reprints and permissions information is available at www.nature.com/reprints.

Publisher's note Springer Nature remains neutral with regard to jurisdictional claims in published maps and institutional affiliations.